HHS Public Access

Author manuscript

Angew Chem Int Ed Engl. Author manuscript; available in PMC 2021 December 01.

Published in final edited form as:

Angew Chem Int Ed Engl. 2021 January 04; 60(1): 351–359. doi:10.1002/anie.202010187.

Hyperfluorescence Imaging of Kidney Cancer Enabled by Renal Secretion Pathway Dependent Efflux Transport

Bujie Du,
Department of Chemistry and Biochemistry, The University of Texas at Dallas, 800 W. Campbell Rd., Richardson, TX 75080 (USA)

Yue Chong,
Department of Chemistry and Biochemistry, The University of Texas at Dallas, 800 W. Campbell Rd., Richardson, TX 75080 (USA)

Xingya Jiang,
Department of Chemistry and Biochemistry, The University of Texas at Dallas, 800 W. Campbell Rd., Richardson, TX 75080 (USA)

Mengxiao Yu,
Department of Chemistry and Biochemistry, The University of Texas at Dallas, 800 W. Campbell Rd., Richardson, TX 75080 (USA)

U-Gling Lo,
Department of Urology, University of Texas Southwestern Medical Center, 5323 Harry Hines Blvd., Dallas, TX 75390 (USA)

Andrew Dang,
Department of Urology, University of Texas Southwestern Medical Center, 5323 Harry Hines Blvd., Dallas, TX 75390 (USA)

Yu-An Chen,
Department of Urology, University of Texas Southwestern Medical Center, 5323 Harry Hines Blvd., Dallas, TX 75390 (USA)

Siqing Li,
Department of Chemistry and Biochemistry, The University of Texas at Dallas, 800 W. Campbell Rd., Richardson, TX 75080 (USA)

Elizabeth Hernandez,
Department of Urology, University of Texas Southwestern Medical Center, 5323 Harry Hines Blvd., Dallas, TX 75390 (USA)

Jason C. Lin,
Department of Chemistry and Biochemistry, The University of Texas at Dallas, 800 W. Campbell Rd., Richardson, TX 75080 (USA)

[*] jiezheng@utdallas.edu .

Conflict of interest

Provisional patent applications related to the studies have been filed.

Jer-Tsong Hsieh,
Department of Urology, University of Texas Southwestern Medical Center, 5323 Harry Hines Blvd., Dallas, TX 75390 (USA)

Jie Zheng*
Department of Chemistry and Biochemistry, The University of Texas at Dallas, 800 W. Campbell Rd., Richardson, TX 75080 (USA)

Department of Urology, University of Texas Southwestern Medical Center, 5323 Harry Hines Blvd., Dallas, TX 75390 (USA)

Abstract

Renal tubular secretion is an active efflux pathway for the kidneys to remove molecules but has yet to be used to enhance kidney cancer targeting. We report indocyanine green (ICG) conjugated with a 2100 Da PEG molecule (ICG-PEG45) as a renal-tubule-secreted near-infrared-emitting fluorophore for hyperfluorescence imaging of kidney cancers, which cannot be achieved with hepatobiliary- and glomerular-clearable ICG. This pathway-dependent targeting of kidney cancer arises from the fact that the secretion pathway enables ICG-PEG45 to be effectively effluxed out of normal proximal tubules through P-glycoprotein transporter while being retained in cancerous kidney tissues with low P-glycoprotein expression. Tuning elimination pathways and utilizing different efflux kinetics of medical agents in normal and diseased tissues could be a new strategy for tackling challenges in disease diagnosis and treatments that cannot be addressed with passive and ligand-receptor-mediated active targeting.

Keywords

indocyanine green; imaging agents; PEGylation; renal cell carcinoma; tumor imaging

Introduction

Upon the interactions with kidney compartments, molecules can take two different pathways, glomerular filtration and renal tubular secretion, to be eliminated through the kidneys[1] (Scheme 1). For some molecules[2] that have little interactions with kidney compartments and are smaller than 6 nm in hydrodynamic diameter (or lower than 40 kDa in molecular weight),[3] they can be rapidly and passively eliminated through the glomerular filtration membrane (Scheme 1a). On the other hand, some other molecules can be actively excreted from peritubular capillaries into the lumen of the proximal tubules by utilizing the transporters on the basolateral side of proximal tubular cells, influx into the cells and efflux from the luminal side[4] (Scheme 1b). The newly developed renal clearable nanofluorophores[5] and organic dyes[2b] are mainly taking the glomerular filtration pathway and have been used for detecting kidney dysfunction[6] or improving positive contrast of many cancers[7] for fluorescence-guided surgery. However, none of them was reported to selectively target primary kidney cancers over normal kidney tissues and “light up” the tumor margins with positive contrast (hyperfluorescence), which is highly demanded in fluorescence-guided partial nephrectomy to preserve kidney function and improve the quality of life of patients with kidney cancer[8] (Scheme 1d). Considering that over

90 percent of kidney cancer is renal cell carcinoma (RCC) originating from the renal tubular epithelial cell[9] (Scheme 1c), the fundamental understanding of the interactions and transport of renal clearable dyes and nanoparticles with/in renal tubules is essential to designing new strategies for selectively targeting of RCC. The renal tubule-secretable fluorophores are particularly interesting because their enhanced interaction with basolateral side of renal tubules allows to fully investigate the correlation between renal transport of nanofluorophores and their ability of selective RCC targeting. However, until now, the renal-tubule-secretable fluorophores, specifically near infrared (NIR)-emitting ones, have not been developed.

Herein, we report the very first renal tubule-secretable NIR-emitting fluorophore. By conjugating Indocyanine green (ICG) with a series of polyethylene glycol (PEG) with molecular weight below 10000 Da, we found that PEG45 (45=the number of repeat ethylene oxide units in PEG; MW, 2100 Da) enabled ICG to be rapidly and actively eliminated almost exclusively through the renal tubular secretion pathway into the urine. The low MW PEGylation prevented ICG from being taken up by the liver while enhancing its interaction with transporters of the proximal tubular cells and allowing ICG to be transported from peritubular capillary to proximal tubular lumen with assistance of organic anion transporters on the basolateral side (“enter in” proximal tubular cells) and P-glycoprotein (P-gP) efflux transporters (“get out” from the proximal tubular cells). Since P-gP efflux transporters are expressed at a much lower level on the membrane of kidney cancer cells than normal proximal tubular cells, ICG-PEG45 was efficiently eliminated out of the normal kidney tissues while being retained in kidney cancerous tissues. In contrast, ICG eliminated through either the liver or glomeruli failed to selectively target kidney cancers over normal kidney tissues due to their limited interactions with transporters of proximal tubules. Not limited to primary kidney cancers, ICG-PEG45 also fluorescently detected extrarenal metastases in bone, brain and lung at high specificity. Combining these findings clearly highlights the importance of tuning elimination pathways and modulating efflux kinetics of medical agents in normal and diseased tissues will open a new path to address long-standing challenges in the diagnosis and treatments of diseases, which are hardly achieved by current passive and ligand-receptor based active strategies.[10]

Results and Discussion

Uniqueness of PEG45 in Altering the Clearance of ICG

The ICG-PEG45 was readily synthesized through the reaction between the N-hydroxysuccinimide (NHS) ester of ICG and the amine group of PEG45 (MW, 2100 Da) molecules (Figure S1). Unreacted ICG and PEG45 were removed through Sephadex-based gel filtration based on their differences in hydrophobicity and size. ICG-PEG45 exhibited the same absorption and photoluminescence properties as free ICG (Figure S2), which allowed in situ fluorescent monitoring of its transport and tumor targeting in the kidneys. While ICG is known to strongly bind proteins, the conjugation of PEG45 molecule significantly reduced the affinity of ICG to serum proteins (Figure S3) because of the dramatically reduced hydrophobicity of ICG-PEG45 ($\log D$=−1.17) compared to that of free ICG ($\log D$=0.68, Figure 1a). Due to the strong serum protein binding, free ICG rapidly

transported into the liver upon intravenous injection, leading to little accumulation in the kidneys and undetectable signal in urine (Figure 1b). In contrast, the conjugation of PEG45 switched the elimination of ICG from the liver to the kidney (Figure 1b). To quantify the differences in clearance pathway of ICG with or without PEG45 conjugation, we collected the feces and urine within 24 hours from the mice with intravenous injection of ICG and ICG-PEG45, respectively. As shown in Figure 1c, 85.3% ID (percentage of injection dose) of free ICG was found in the feces, which is 29.8 times higher than ICG-PEG45 (2.9% ID) while free ICG was undetectable in the urine and 92.9% ID of ICG-PEG45 was found in urine within 24 h post injection. Combining in vivo imaging and *ex vivo* clearance studies indicates that the conjugation of PEG45 nearly completely switched the elimination pathway of ICG from the hepatic clearance to the renal clearance. In addition to PEG45 (MW, 2100 Da), PEG22 (MW, 1100 Da) and PEG220 (MW, 10100 Da) were also conjugated to ICG, respectively. ICG-PEG22 and ICG-PEG220 retained the same absorption and photoluminescence properties as free ICG (Figure S4) and allowed us to conduct fluorescence imaging of in vivo transport and ex vivo tissue distribution (Figure S5). By quantifying ICG amount in feces and urine, we discovered two unique MW-dependent scaling laws in the hepatobiliary and renal clearance (Figure 1d). First, the amount of ICG in feces decreased with the increase of PEG molecular weight, which strongly correlated with their MW-dependent resistance to serum proteins (Figure S6). Second, the renal clearance efficiencies of ICG-PEG22 (28.9% ID) and ICG-PEG220 (44.9%ID) were both lower than that of ICG-PEG45, clearly showing the uniqueness of PEG45 in tailoring the renal clearance of ICG. This MW-dependent scaling law of renal clearance, in which PEG45 (MW=2100 Da) is an optimized MW to generate the most efficient renal clearance for ICG, is consistent with our previously observed one from renal clearable fluorophore IRDye800CW[11] and further elucidates the high sensitivity and unique responses of the kidneys to molecules with subtle differences in size.[11]

Renal Tubular Secretion of ICG-PEG45

PEGylated organic dyes such as IRDye800CW, ZW8001 and fluorescein have been found to clear out of the kidneys through the glomerular filtration.[11] To understand how ICG-PEG45 is eliminated through the kidneys, we first used in vivo fluorescence imaging to noninvasively monitor the kidney clearance kinetics of ICG-PEG45. Interestingly, the fluorescent signal of ICG-PEG45 in the kidneys rapidly reached its maximum at ≈5 post intravenous injection (p.i.) and remained a plateau within 30 min time period (Figure 1e). This phenomenon was distinct to the observation of glomerular filtrated PEGylated organic dyes, such as IRDye800CW-PEG45 (800CW-PEG45),[11] of which fluorescent signal from the kidneys reached the peak at ≈2 min p.i., followed by a rapid decay within 30 min (dot line in Figure 1e). This plateau of ICG-PEG45 signal in the kidneys was still observed within 30 min p.i. even when the injection dose was reduced by 10 times (Figure S7), suggesting that the elimination of ICG-PEG45 rapidly reached equilibrium in an early phase and the elimination kinetics was actively controlled by the kidney compartments. The plateau of ICG-PEG45 in the kidneys gradually disappeared after one hour and was followed by a descending phase (Figure S8), consistent with that ICG-PEG45 was eventually eliminated through the kidneys into the urine.

To unravel the origin of the unique time-dependent kidney fluorescence curve of ICG-PEG45, we harvested the kidneys from the mice intravenously injected with ICG-PEG45 at 5 min, 10 min and 1 h p.i. and then studied their distribution in the kidneys with fluorescence microscopy imaging. At 5 min (Figure 1 f, right) and 10 min (Figure S9) p.i., the fluorescence signals of ICG-PEG45 dominantly located in the peritubular capillaries, ≈4.5 times and ≈8.5 times higher than those of glomeruli and proximal tubules, respectively (Figure S10a). In contrast, 800CW-PEG45 (Figure 1 f, left) mainly located in the glomeruli and luminal side of proximal tubules at 5 min due to rapid glomerular filtration and its rapid renal clearance resulted in a very weak signal from the kidneys at 1 h p.i. Distinctly, at 1 h p.i., the peritubular space's signal of ICG-PEG45 decreased and the glomeruli remained dark, but the luminal side of the proximal renal tubules became much more distinguishable (Figure 1 f and Figure S10b). The distinct kidney distribution of ICG-PEG45 from 800CW-PEG45 suggested different kidney elimination pathways and ICG-PEG45 could be directly cleared into urine through transportation from the peritubular capillary (PTC) into the tubularinterstitum (TI) and finally reached the proximal tubular lumen, the process of renal tubular secretion (as shown in Scheme 1b).

To further confirm the mechanism of active renal tubular secretion of ICG-PEG45 at the molecular level, we treated the mice with probenecid, an organic anion transporter inhibitor, [12] to inhibit the renal basolateral uptake process without alteration of glomerular filtration (Figure S11). As control, 800CW-PEG45 was also investigated under same probenecid treatment. As shown in Figure 1g, the administration of probenecid significantly reduced the renal clearance efficiency of ICG-PEG45 at 30 min p.i. but did not influence the clearance of 800CW-PEG45, indicating the involvement of organic anion transporter-dependent active tubular secretion in the kidney transport of ICG-PEG45. The differences in the kidney elimination pathways between 800CW-PEG45 and ICG-PEG45 are closely related to the inherent properties of the parent molecules since free 800CW has no specific interactions with the body and was rapidly filtered through the glomeruli, whereas free ICG is known to bind to a variety of organic anion transporters.[13] The observed renal tubular secretion of ICG after conjugation of PEG45 suggested that PEG45 enhanced the affinity of ICG to organic anion transporters on the basolateral side of proximal tubular cell (Figure 1h) while reducing its affinity to the transporters involved in the hepatobiliary clearance. These findings highlight that the synergistic effect of conjugation of low-MW PEGylation to the ICG with high affinity to transporters could lead to a new molecular interaction, cellular influx and efflux mechanism, and elimination pathway, which have never been observed from any known organic dyes before.[14]

Hyperfluorescent Imaging of Primary Kidney Cancers with ICG-PEG45

The novel renal tubular secretion pathway of ICG-PEG45 made it possible to investigate whether the renal cell carcinoma, originating from the renal tubules, can be targeted by the molecules with strong interaction with proximal tubules. We firstly established orthotopic xenograft model of papillary RCC (pRCC), one type of RCC that is difficult to be targeted by both passive targeting agent (such as ICG) and active targeting agent (such as ^{111}In-DOTA-girentuximab-IRDye800CW,[14] ^{18}F-FB-mini-PEG-E[c(RGDyK)][15]) due to its low expression of carbonic anhydrase IX (CAIX) or integrin.[16] The papillary RCC

cell line (ACHN), transfected with luciferase-expression vector, were surgically implanted into subcapsular space of the left kidney of mice and the right kidney was kept normal for renal function (Figure 2a). When the RCC tumor developed to a size that can be reliably detected in the left kidney by bioluminescent imaging, we intravenously injected ICG-PEG45 into the mice and then conducted noninvasive in vivo fluorescence imaging. As shown in Figure 2b and c, the fluorescence intensity observed from the contralateral right kidney initially (≈within 1–5 hours) was higher than that from left kidney with pRCC because ICG-PEG45 rapidly transported through the normally functionalized right kidney. As ICG-PEG45 was gradually eliminated through the right normal kidney, the fluorescence intensity observed from the left kidney with pRCC became higher than the contralateral one over time. We also quantified the clearance percentage of the peak intensity of kidneys at 24 h (defined as [peak value-intensity at 24 h]/peak value]×100%) and found that the value of left pRCC kidney is is 29.86±3.12%, which is 2.18 times lower than that of contralateral kidney (65.15±5.09%) (Figure 2d), suggesting the long retention of ICG-PEG45 in the pRCC kidney in comparison with normal kidney. Ex vivo fluorescence imaging of these two kidneys at 24 h post injection (Figure 2e) further confirmed that the prolonged retention of ICG-PEG45 in the pRCC kidney specifically occurred in tumor regions: the fluorescence intensity of ICG-PEG45 in the cancerous kidney tissues is higher than that in the normal contralateral kidney, clearly indicating that ICG-PEG45 was capable of hyperfluorescently lighting up pRCC cancerous tissue and also differentiating the tumor-to-normal tissue borders. By further localizing the distribution of ICG-PEG45 in the pRCC tissue using fluorescence microscope (Figure 2 f), we observed that ICG-PEG45 was taken up by kidney cancer cells, clearly indicating that ICG-PEG45 can selectively target kidney cancer cells. Not limited to pRCCs, ICG-PEG45 also hyperfluorescently lighted up clear cell RCCs (ccRCCs) in the patient-derived xenograft (PDX) model and successfully differentiated the tumor-to-normal tissue borders (Figure 2g), indicating the generalizability of ICG-PEG45 in detection of multiple types of RCCs.

As control, we also investigated the kidney cancer targeting of free ICG (cleared through the hepatobiliary clearance) and 800CW-PEG45 (cleared through the glomerular filtration), which neither can reach the basolateral side of proximal tubules. As shown in Figure S12, both of them failed to hyperfluorescently light up RCC in the kidneys and the contrast indexes of the tumor regions were 0.95 and 0.33 (hypofluorescent) for ICG and 800CW-PEG45, respectively, which is 1.59 times and 4.58 times lower than that of ICG-PEG45 (Figure 2h). Moreover, the ICG was also conjugated onto renal clearable glutathione coated Au25 clusters to enhance its glomerular filtration in the kidneys[17] but we found that it still failed to selectively target primary kidney cancers over normal kidney tissues (Figure S13). This further confirms that kidney cancer targeting of ICG is strongly dependent of its elimination pathway in the kidneys (Figure 2i) and the renal tubular secretion pathway allows ICG to target cancerous tubule cells through the basolateral side of proximal tubules.

Distinct Efflux Transport Kinetics of ICG-PEG45 in Normal and Cancerous Kidney Cells

Based on the mechanism of renal tubular secretion, the cellular efflux of molecules from the proximal tubular cells into proximal tubular lumen is dictated by the efflux transporters located on the apical membrane of the proximal tubular cells, which behave as a pump

to eliminate exogenous substances and dictate the intracellular drug accumulation.[18] P-glycoprotein (P-gP) efflux transporter[19] is well known to involve in transport of many organic molecules in the renal tubular secretion. By quantifying P-gP expression level on normal proximal tubular cells (HK2), papillary renal cancer cells (ACHN) as well as its expression level on normal kidney tissue and papillary renal cancerous tissue (ACHN tumor) with western blot analysis (Figure 3a), we found that the expression of P-gP efflux transporter in renal cancerous tissue at both cellular and tissue level was significantly lower than that in normal proximal tubular cell and normal kidney tissues, consistent with reported literature.[20] Thus, we hypothesized that the long retention of ICG-PEG45 in kidney cancerous tissue might be closely related to their low expression of P-gP efflux transporter.

To validate our hypothesis and unravel the selective targeting of ICG-PEG45 to kidney cancers at the molecular level, we investigated in vitro cellular retention of ICG-PEG45 in HK2 and ACHN before and after P-gP inhibitor treatment. After being incubated with ICG-PEG45 for 1 h at 378C, both normal and cancer cells were washed with cold HEPES buffer to remove free ICG-PEG45 in the medium and the fluorescence intensities of both cells were quantified using a fluorescent microscope. As shown in Figure 3b, ICG-PEG45 was efficiently taken up by both cell lines; but the average emission intensity of papillary RCC cells was ≈1.52 times higher than that of HK2 cells (Figure 3c). Once we treated cells with cyclosporin A (CSA), an inhibitor of P-gP (Figure 3b and c), we found that the treatment of CSA obviously increased the intensity of ICG-PEG45 in normal HK2 cells but did not significantly influence the intensity of ICG-PEG45 in the RCC ACHN cell line, confirming that the P-gP efflux transporter was indeed involved in the secretion of ICG-PEG45 from normal proximal tubular cells. In addition, this finding also suggests that the efflux of ICG-PEG45 in renal cancer cells was compromised compared to that in the normal kidney tubular cells due to low expression of P-gP efflux transporter. Moreover, when efflux was inhibited by CSA treatment, normal kidney tubular cell HK2 and kidney cancerous cell ACHN showed no significant difference in fluorescence intensity, indicating that uptake efficiencies of ICG-PEG45 by normal and cancerous kidney cells were comparable. Therefore, the observed difference in the fluorescence intensity between normal and cancerous kidney without CSA treatment is due to the difference in efflux kinetics of ICG-PEG45. To further confirm the role of P-gP transporter in mediating the intracellular accumulation of ICG-PEG45, another specific P-gP inhibitor, tariquidar, was also applied to HK2 and ACHN cells under same conditions and same results as CSA treatment were observed (Figure S14). These findings confirmed that the difference in the efflux kinetics of ICG-PEG45 between normal kidney and cancerous tissues, governed by P-gP efflux transporter, is responsible for its selective retention in kidney tumors (Figure 3d). This finding not only illustrates the uniqueness of ICG-PEG45 in hyperfluorescent detecting of renal cell carcinoma at the molecular level but also provides a new strategy for cancer detection and targeting by taking advantage of the inherent difference in the cellular efflux of imaging agents in normal and cancerous tissue, distinct to the conventional passive targeting mechanism as well as ligand-receptor mediated active targeting strategy that have been widely used in the cancer detection through enhancing affinity of probes to cancer receptors.

ICG-PEG45 Selectively Detects RCC Metastasis at High Specificity

Not limited to primary RCC, we also found that ICG-PEG45 successfully detected RCC metastases in other organs such as brain, bone and lung[21] in the mouse model (Figure 4a). As shown in Figure 4b, the metastatic tumors near the spine and brain were confirmed with bioluminescence and the tumor in spine can be noninvasively detected through the fluorescence of ICG-PEG45. Although the metastatic tumors in brain cannot noninvasively be observed by the fluorescence of ICG-PEG45 due to the skull, the ex vivo fluorescence imaging (Figure 4c) clearly implied the ability of ICG-PEG45 in targeting the RCC metastatic tumors in brain. More importantly, very small tumor nodules in the bones of limbs, which cannot be detected with bioluminescence (Figure 4d) but confirmed by H&E pathology images (Figure 4 f), were also readily detected by the fluorescence of ICG-PEG45 (Figure 4d and Figure 4e) with a contrast index of 2.28±0.13, ≈2 times higher than that of normal joints without tumor (Figure S15). In addition to the RCC metastasis in brain and bone, its metastatic tumors in lungs also can be fluorescently imaged (Figure S16). These results clearly showed that low-MW PEG45 endowed ICG the functionality in detection of RCC metastasis with positive contrast and high specificity.

Conclusion

In conclusion, using simple low MW PEGylation chemistry (PEG45, 2100 Da), we enabled a well-known clinically approved NIR-emitting fluorophore, ICG, to be rapidly and actively secreted into urine through the normal proximal tubules in the kidneys while being retained in the kidney cancerous tissues. As a result, ICG-PEG45 can hyperfluorescently detect kidney tumors, a long-standing challenge in the fluorescence-guided partial nephrectomy, which cannot be readily achieved with either hepatobiliary or glomerular clearable ICG or other renal clearable fluorophores. Different from well-known passive and ligand-receptor mediated active targeting strategies, such unique tumor targeting of ICG-PEG45 fundamentally arises from this novel renal secretion pathway: on one hand, it enables ICG-PEG45 to be efficiently taken up by both normal and cancerous proximal tubules through the organic anion transporter on the basolateral side; on the other hand, taking advantage of differences in the expression level of P-gP efflux transporter between normal and cancerous kidney cells, it enables ICG-PEG45 to selectively accumulate in the kidney cancerous tissue while being efficiently eliminated from the normal kidney tissues. Not limited to primary kidney cancers, extrarenal metastasis can also be fluorescently detected with ICG-PEG45 at high specificity. Since this tubule secretable ICG-PEG45 can be further conjugated with a variety of other imaging tracers and therapeutic agents, its derivatives are expected to significantly advance multimodality imaging (fluorescence imaging integrated with MRI, PET, photoacoustics, CT, etc.) as well as combination therapy (photothermal/photodynamic/chemo/immune/radiation therapies) of kidney and other diseases, which are currently being investigated.

Supplementary Material

Refer to Web version on PubMed Central for supplementary material.

Acknowledgements

This study was supported by National Institutes of Health (NIH) (R01DK103363 and R01DK115986), Cancer Prevention Research Instituted of Texas (CPRIT) (RP200233), Welch Research Foundation (AT-1974-20180324) and Cecil H. and Ida Green Professorship of J.Z. from the University of Texas at Dallas.

References

[1]. Hall JE, Guyton and Hall Textbook of Medical Physiology E-Book: with STUDENT CONSULT Online Access, Elsevier Health Sciences, 2010.

[2]. a) Jorgensen K, Møller J, Sheikh M, Acta Physiol. Scand 1972, 84, 408–414; [PubMed: 5019037] b) Choi HS, Nasr K, Alyabyev S, Feith D, Lee JH, Kim SH, Ashitate Y, Hyun H, Patonay G, Strekowski L, Angew. Chem. Int. Ed 2011, 50, 6258–6263; Angew. Chem. 2011, 123, 6382–6387;c) Sykes EA, Chen J, Zheng G, Chan WC, ACS Nano 2014, 8, 5696–5706; [PubMed: 24821383] d) Du B, Jiang X, Das A, Zhou Q, Yu M, Jin R, Zheng J, Nat. Nanotechnol 2017, 12, 1096. [PubMed: 28892099]

[3]. a) Haraldsson B, Nystrçm J, Deen WM, Physiol. Rev. 2008, 88, 451–487; [PubMed: 18391170] b) Du B, Yu M, Zheng J, Nat. Rev. Mater. 2018, 3, 358–374.

[4]. a) Morrissey KM, Stocker SL, Wittwer MB, Xu L, Giacomini KM, Annu. Rev. Pharmacol. Toxicol 2013, 53, 503–529; [PubMed: 23140242] b) Wang K, Kestenbaum B, Clin. J. Am. Soc. Nephrol 2018, 13, 1291–1296. [PubMed: 29490976]

[5]. a) Burns AA, Vider J, Ow H, Herz E, Penate-Medina O, Baumgart M, Larson SM, Wiesner U, Bradbury M, Nano Lett. 2009, 9, 442–448; [PubMed: 19099455] b) Choi HS, Liu W, Misra P, Tanaka E, Zimmer JP, Ipe BI, Bawendi MG, Frangioni JV, Nat. Biotechnol. 2007, 25, 1165–1170; [PubMed: 17891134] c) Zhou C, Long M, Qin Y, Sun X, Zheng J, Angew. Chem. Int. Ed 2011, 50, 3168–3172; Angew. Chem. 2011, 123, 3226–3230.

[6]. a) Yu M, Zhou J, Du B, Ning X, Authement C, Gandee L, Kapur P, Hsieh JT, Zheng J, Angew. Chem. Int. Ed 2016, 55, 2787–2791; Angew. Chem. 2016, 128, 2837–2841;b) Huang J, Li J, Lyu Y, Miao Q, Pu K, Nat. Mater 2019, 18, 1133–1143. [PubMed: 31133729]

[7]. a) Bradbury MS, Phillips E, Montero PH, Cheal SM, Stambuk H, Durack JC, Sofocleous CT, Meester RJ, Wiesner U, Patel S, Integr. Biol 2013, 5, 74–86;b) Choi HS, Gibbs SL, Lee JH, Kim SH, Ashitate Y, Liu F, Hyun H, Park G, Xie Y, Bae S, Nat. Biotechnol 2013, 31, 148; [PubMed: 23292608] c) Kang H, Rho S, Stiles WR, Hu S, Baek Y, Hwang DW, Kashiwagi S, Kim MS, Choi HS, Adv. Healthcare Mater 2020, 9, 1901223.

[8]. Navaratnam A, Abdul-Muhsin H, Humphreys M, F1000Research 2018, 7, 1948.

[9]. Ricketts CJ, Linehan WM, Cell 2018, 173, 540–542. [PubMed: 29677504]

[10]. a) Sindhwani S, Syed AM, Ngai J, Kingston BR, Maiorino L, Rothschild J, MacMillan P, Zhang Y, Rajesh NU, Hoang T, Nat. Mater 2020, 19, 566; [PubMed: 31932672] b) Zhou Q, Shao S, Wang J, Xu C, Xiang J, Piao Y, Zhou Z, Yu Q, Tang J, Liu X, Nat. Nanotechnol 2019, 14, 799–809. [PubMed: 31263194]

[11]. Du B, Jiang X, Huang Y, Li S, Lin JC, Yu M, Zheng J, Bioconjugate Chem 2019, 31,241–247.

[12]. Takahara N, Saga T, Inubushi M, Kusuhara H, Seki C, Ito S, Oyama N, Yokoyama O, Sugiyama Y, Fujibayashi Y, Nucl. Med. Biol 2013, 40, 643–650. [PubMed: 23618840]

[13]. Shibasaki Y, Morita Y, Sakaguchi T, Konno H, in ICG Fluorescence Imaging and Navigation Surgery, Springer, 2016, pp. 351–362.

[14]. Hekman MC, Rijpkema M, Muselaers CH, Oosterwijk E, Hulsbergen-Van de Kaa CA, Boerman OC, Oyen WJ, Langenhuijsen JF, Mulders PF, Theranostics 2018, 8, 2161. [PubMed: 29721070]

[15]. Withofs N, Signolle N, Somja J, Lovinfosse P, Nzaramba EM, Mievis F, Giacomelli F, Waltregny D, Cataldo D, Gambhir SS, J. Nucl. Med 2015, 56, 361–364. [PubMed: 25655629]

[16]. An H-W, Hou D, Zheng R, Wang M-D, Zeng X-Z, Xiao W-Y, Yan T-D, Wang J-Q, Zhao C-H, Cheng L-M, ACS Nano 2020, 14, 927–936. [PubMed: 31927974]

[17]. Jiang X, Du B, Zheng J, Nat. Nanotechnol 2019, 14, 874–882. [PubMed: 31308501]

[18]. Yin J, Wang J, Acta Pharm. Sin. B 2016, 6, 363–373. [PubMed: 27709005]

[19]. Koziolek MJ, Riess R, Geiger H, Thévenod F, Hauser IA, Kidney Int. 2001, 60, 156–166. [PubMed: 11422747]

[20]. Nishiyama K, Shirahama T, Yoshimura A, Sumizawa T, Furukawa T, Ichikawa-Haraguchi M, Akiyama SI, Ohi Y, Cancer 1993, 71, 3611–3619. [PubMed: 8098269]

[21]. Gong J, Maia MC, Dizman N, Govindarajan A, Pal SK, Asian J. Urol 2016, 3, 286–292. [PubMed: 29264197]

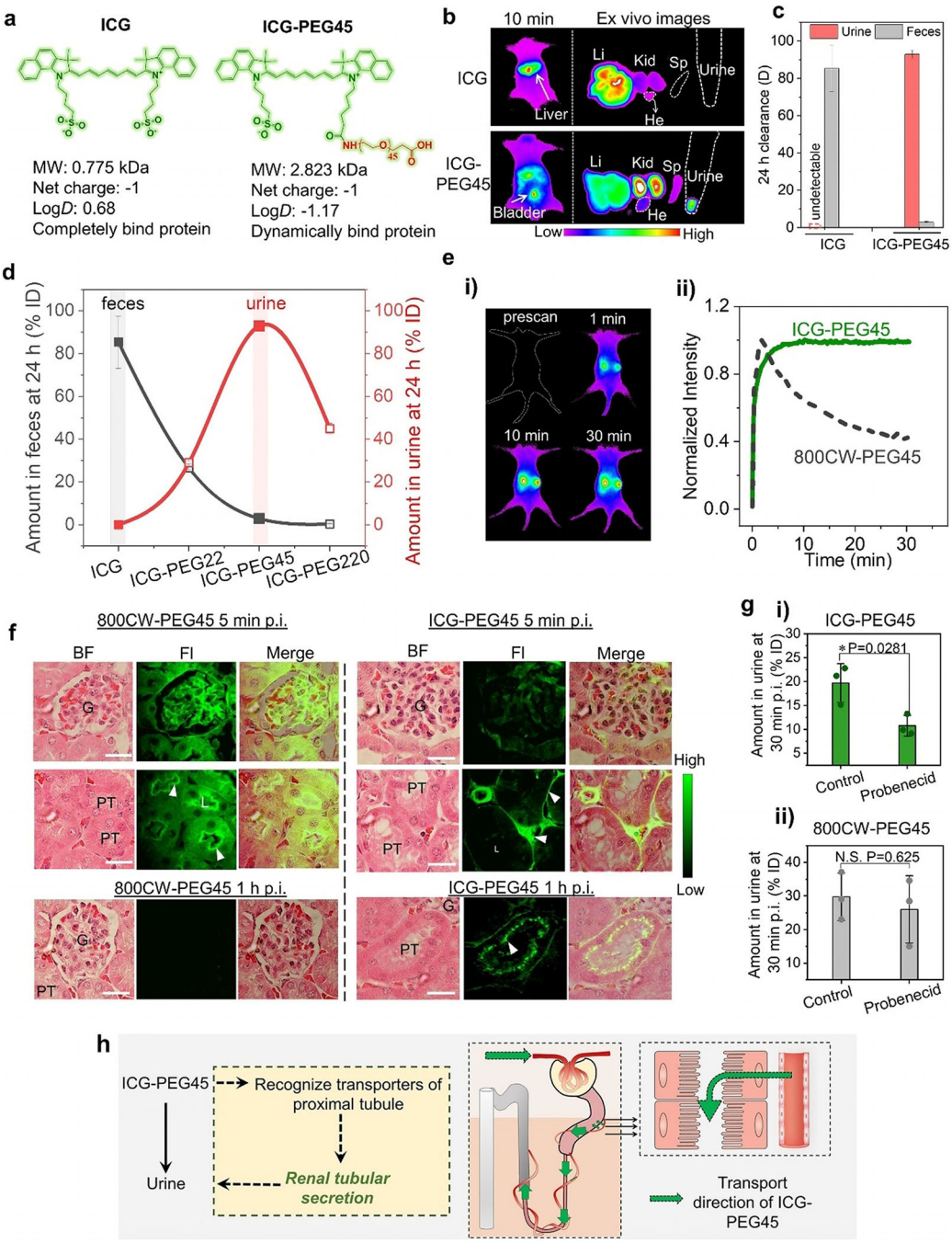

Figure 1.

PEG45 switches the clearance pathway of ICG from hepatobiliary clearance to renal tubular secretion. a) Comparison between ICG and ICG-PEG45 in chemical structures, molecular weight (MW), net charge, partition coefficient (log*D*), and serum protein binding. b) *In vivo* imaging of mice intravenously injection of ICG and ICG-PEG45 at 10 min post injection and ex vivo images of harvested liver (Li), kidneys (Kid), heart (He), spleen (Sp) and urine collected from bladder at 10 min post intravenous injections (Ex/Em filters: 790/830 nm). The mice were placed in prone position to collect signals from the liver.

c) Clearance percentage of ICG and ICG-PEG45 in urine and feces, respectively, at 24 h post intravenous injection. d) Clearance percentage of ICG, ICG-PEG22, ICG-PEG45 and ICG-PEG220 in feces and urine at 24 h post injections. n=3. PEG45 behaved as a turning point in terms of renal clearance of ICG-PEGn. e) Real-time noninvasive kidney imaging before and after intravenous of injection of ICG-PEG45 (Ex/Em filters: 790/830 nm; i) and time-fluorescence intensity curves of two kidneys within 30 min post injection of ICG-PEG45 (ii). To make a comparison, the fluorescent kidney kinetics curve of 800CW-PEG45 was presented in the dotted line. To collect the signals of the kidneys, the mouse was placed in supine position on the imaging stage. f) Fluorescence images of glomerulus and tubules at tissue level at 5 min and 1 h post injection of 800CW-PEG45 and ICG-PEG45. G, glomerulus, PT, proximal tubule. Kidney tissue was stained by Hematoxylin and Eosin (H&E). Fluorescence images were taken at 775/845 nm for ICG-PEG45 and 720/790 nm for 800CW-PEG45. Scalar bar is 20 μm. g) The renal clearance efficiencies of ICG-PEG45 (i) and 800CW-PEG45 (ii) at 30 min post injection under control condition and probenecid-treated condition. n=3. *represents statistically different based on student t-test, P<0.05. N.S. represents no significant difference based on student-test, P>0.05. h) The schematic diagrams of the clearance alteration of ICG after conjugation of PEG45.

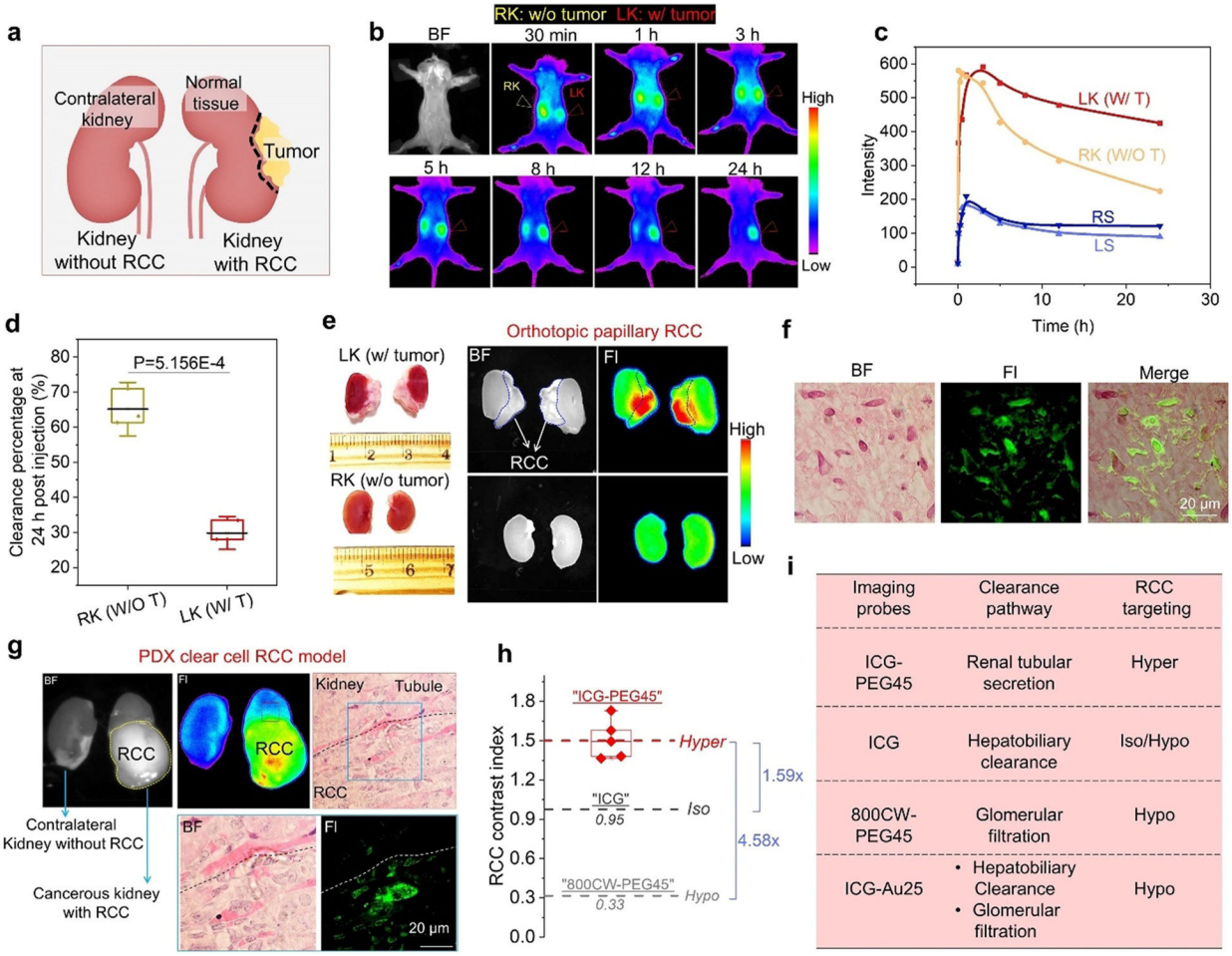

Figure 2.

Hyperfluorescent imaging of primary kidney cancers with ICG-PE45. a) The schematic diagrams of an established mouse model primary, orthotopic renal cell carcinoma (RCC). b) Real-time noninvasive kidney imaging of orthotopic papillary RCC implanted mice after intravenous injection of ICG-PEG45 (Ex/Em filters: 790/830 nm). BF, bright field. Left kidney of mice was implanted with RCC (LK: w/tumor) and right kidney was normal kept (RK: w/o tumor). The mouse was placed in supine position on the imaging stage. c) Time-fluorescence intensity curves of two kidneys locations and background skin within 24 h post injection of ICG-PEG45. RS, right background skin. LS, left background skin. d) Clearance percentage of at 24 h post injection of ICG-PEG45 of RK (w/o T) and LK (w/T). The value was defined as [peak value-intensity at 24 h]/peak value] ×100%. n=3, p value was calculated based on student t-test. e) Ex vivo images of cancerous kidney with papillary RCC (LK) and contralateral kidney without RCC (RK) at 24 h post intravenous injection of ICG-PEG45. f) The distribution of ICG-PEG45 in papillary RCC tissue at 24 h post injection. g) Ex vivo images of cancerous kidney with patient-derived xenograft (PDX) clear cell RCC (ccRCC) and contralateral kidney without RCC at 68 h post injection of ICG-PEG45 and fluorescence imaging of tissue level after H&E staining. BF, bright field. Fl, fluorescence from ICG-PEG45. The dot line represents the margin between normal kidney tissue and ccRCC. h) The comparison of RCC contrast index among ICG-PEG45,

ICG and 800CW-PEG45. Hypo, hypofluorescent (intensity of normal kidneys > intensity of kidney cancer). Iso, isofluorescent (intensity of normal kidneys=intensity of kidney cancer). Hyper, hyperfluorescent (intensity of normal kidneys < intensity of kidney cancer). i) The correlation of clearance pathways with RCC targeting by summarizing investigated probes.

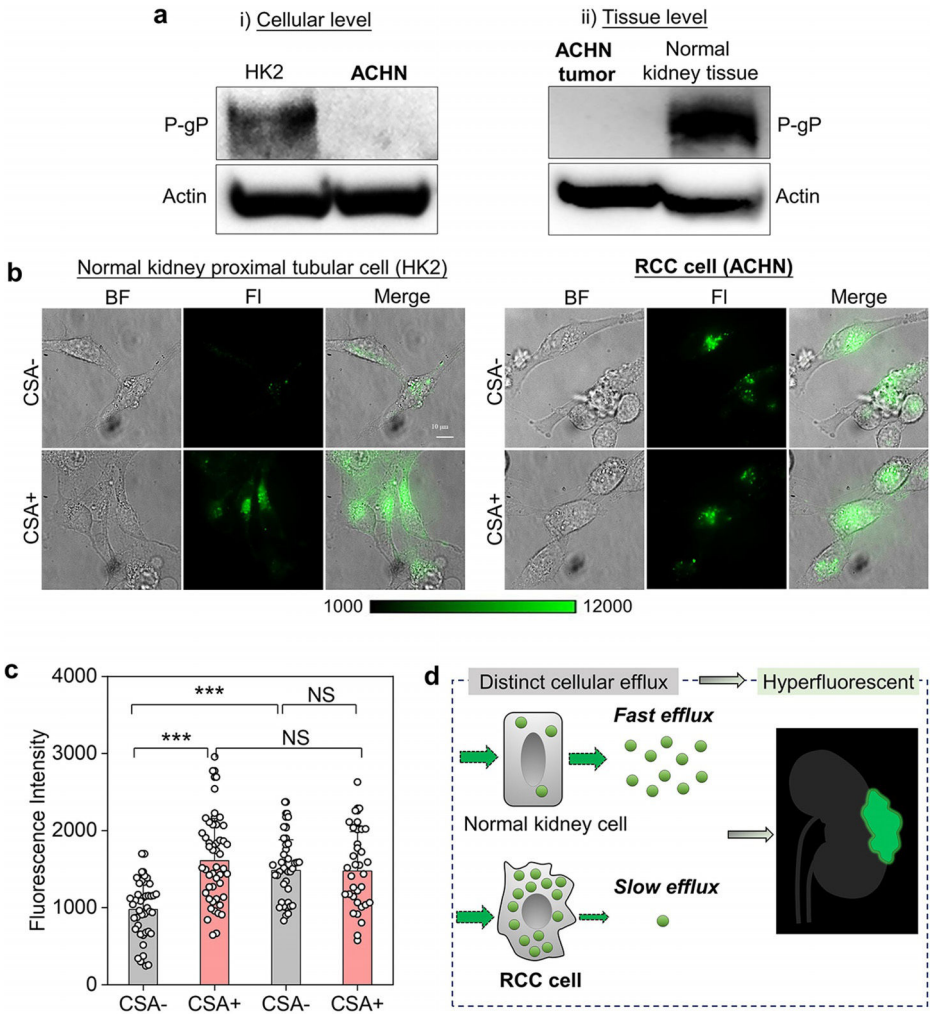

Figure 3.

Distinct efflux transport kinetics of ICG-PEG45 in normal and cancerous kidney cells. a) The P-glycoprotein (P-gP) expression level on the membrane of normal kidney proximal tubular cell (HK2) and renal cell carcinoma cell (ACHN) as well as at the tissue level. Actin was used as internal loading control. b) The cellular uptake fluorescence imaging of ICG-PEG45 in HK2 and ACHN before (CSA−) and after (CSA+) inhibition of P-gP-mediated efflux by the cyclosporin A (CSA) treatment. scalar bar is 10 mm. BF, bright field. Fl, fluorescence. c) The quantification of intracellular fluorescence intensity of ICG-PEG45. *** represents statistically different based on student t-test and $P<0.0005$. N.S. represents no significant difference based on student-test, $P>0.05$. d) The schematic diagrams of distinct cellular efflux of ICG-PEG45 in normal kidney proximal tubular cell and RCC cell, which is the origin of RCC hyperfluorescent contrast by ICG-PEG45.

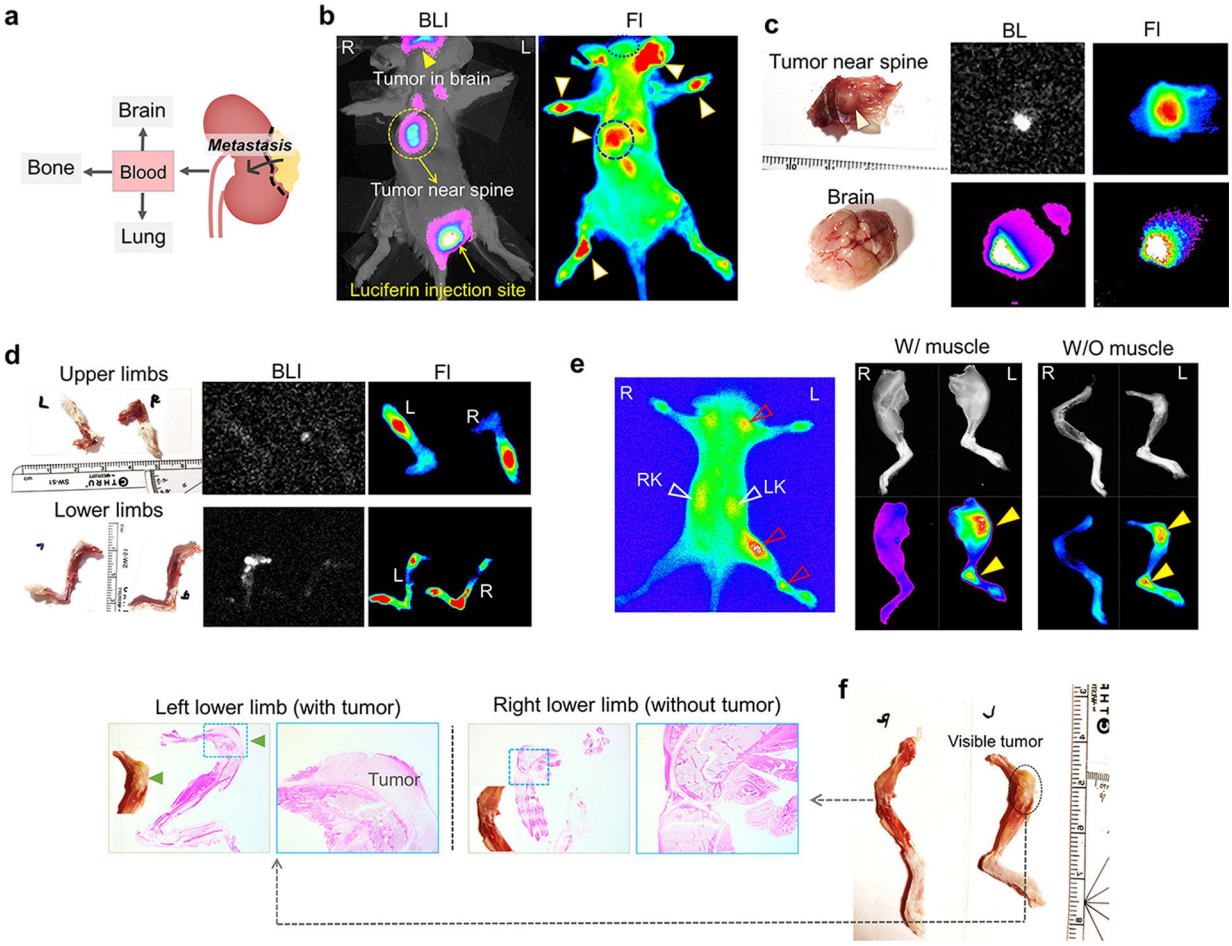

Figure 4.

ICG-PEG45 detects RCC metastasis with high specificity. a) RCC could metastasize to brain, bone and lung. b) In vivo noninvasive bioluminescence images and fluorescence images of mice bearing RCC metastatic tumors at 24 h after injection ICG-PEG45. BLI, bioluminescence images. Fl, fluorescence. R, right, L, left. c) Ex vivo images of tumor near spine and brain at 24 h post injection of ICG-PEG45. BLI, bioluminescence images. Fl, fluorescence. d) Ex vivo images of upper limbs and lower limbs at 24 h post injection of ICG-PEG45. BLI, bioluminescence images. Fl, fluorescence. e) (left) In vivo noninvasive images of other mice bearing RCC metastatic tumors at 24 h post injection of ICG-PEG45. (right) Ex vivo FL images of lower limbs (with and without muscle) and color images (without muscle; f) at 24 h post injection of ICG-PEG45 as well as H&E pathology images. The images of upper limbs were in Figure S17.

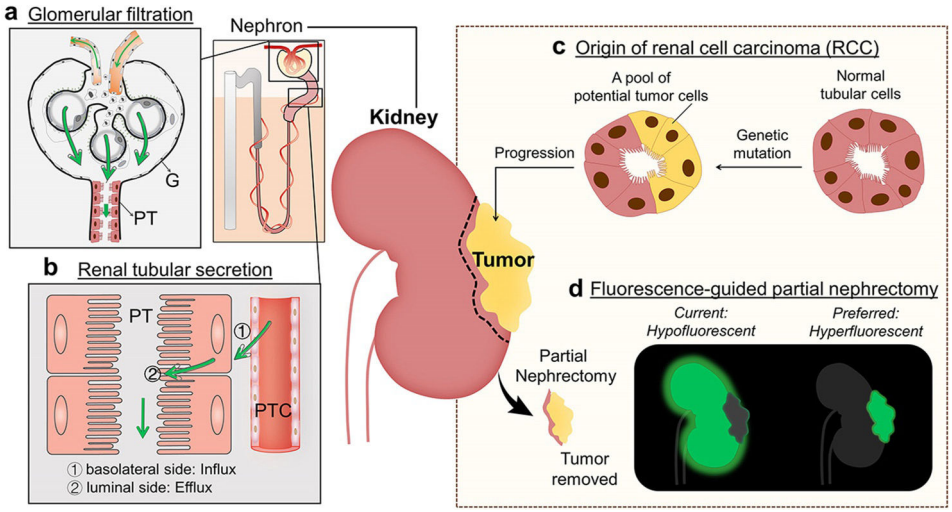

Scheme 1.

Two distinct renal clearance pathways in the kidneys as well as renal cell carcinoma (RCC) targeting of fluorescent agents. a) Glomerular filtration happens at the glomeruli (G) and is a passive, non-specific process to eliminate molecules and nanoparticles from glomerular capillaries to Bowman's space as long as their sizes are below the kidney filtration threshold (≈6 nm or 40 kDa). The filtrated molecules are then transported into bladder by travelling through the renal tubules of the nephrons such as proximal tubules (PT). b) The renal tubular secretion is an active, specific process for removal of small molecules from peritubular capillary (PTC) to renal tubular lumen through 1) binding of the molecule to the transporters on the basolateral side of tubular cells, influx into the cells and 2) efflux from the luminal side of tubular cells. Arrows indicate the direction of transport of exogenous substances. c) RCC originates from the renal tubular epithelial cells because of genetic mutation. d) For fluorescent-guided partial nephrectomy for RCC, fluorescent agents that selectively target kidney cancers over normal kidney tissues (hyperfluorescent) are preferred to improve the precision of tumor removal and preservation of kidney functions. However, most of current agents, especially for passive targeting agent, are retained in and light up normal kidney tissue, resulting in hypofluorescent imaging of primary RCC.